HIGH Q, PRECISION SC CUT RESONATORS WITH LOW ACCELERATION SENSIVITY

R. B. Haskell, P. E. Morley, and D.S. Stevens
Vectron International-Hudson, 267 Lowell Rd., Hudson, NH 03051

*Abstrac*t - **A new mounting structure has enabled the construction of high Q resonators with very low acceleration sensitivity. Values in the range of mid parts in 10^{11} to low parts in 10^{10} per g have been achieved with a simple planar support structure. Utilizing a thin chemically etched lead-frame, a four-point mount with built in stress relief has been designed to mount in the plane of the resonator. The advantages of this structure include good symmetry, minimal residual manufacturing stresses, and minimal asymmetric vibratory stresses. Many different configurations have been designed and built using 8 and 10mm 10MHz 3rd overtone SC cut plano-convex crystals with excellent results.**

***Keywords* – acceleration, sensitivity, g-sensitivity, vibration, quartz, crystal, resonator, QRM**

I. INTRODUCTION

When a resonator is placed in a vibrating environment, the frequency of the resonator will be perturbed as a function of the vibration level. This degrades the stability of the resonator, and can compromise the performance of the system in which it is used.

The acceleration sensitivity of a resonator arises from forces imparted on the crystal element from the surrounding enclosure. These forces are transferred to the crystal through the mount structure. Rigidity and asymmetry of the mounting clips, manufacturing imperfections, and acoustic mode offset can all result in a larger value of observed acceleration sensitivity.

One of the most important factors in achieving reproducibly low acceleration sensitivity is the symmetry of the applied stress field with respect to the acoustic mode center. To a first order approximation, Tiersten and Zhou theoretically showed that for a plano-convex resonator with perfectly aligned acoustic mode and symmetric support centers, the effect of the intrinsic asymmetry due to the contour is a few parts in 10^{12} per g acceleration sensitivity[1]. They also showed that the normal acceleration sensitivity increases linearly with offset of the centers [1-3]. This is a very important result because it stresses the importance of maintaining a very symmetric mount.

The importance of alignment of the mount and acoustic mode centers is further stressed by the work done by EerNisse et al [5-7]. Their approach was to move the acoustic mode center by selectively altering the distribution of mass on the resonator surface. This resulted in a repositioning of the acoustic mode center and a corresponding improvement in acceleration sensitivity.

Another effect that has not been explored in detail is the effect of residual static stresses on acceleration sensitivity. The majority of existing theory assumes that the resonator has a zero dc stress bias when the analysis is performed. In reality, residual stresses caused by annealing of the clips, shrinkage or expansion of the adhesive, and manufacturing imperfections will alter the distribution and symmetry of the applied stress field. Because the applied stress may no longer be aligned with respect to the acoustic mode, there is an effective asymmetry that will result in greater acceleration sensitivity.

One approach to reducing these biasing stresses, as well as reducing the coupling of vibratory stresses, would be to use a compliant mounting structure. Weglein showed that low values of acceleration sensitivity could be achieved by using a visco-elastic adhesive for attaching the crystal to four rectangular mounting posts [8]. Total Γ values = 3 x 10^{-10} per g were reproducibly achieved for 100MHz, 5th overtone resonators. The advantages of this technique are two-fold. First, any residual stresses due to manufacturing will relax in the compliant adhesive. Secondly, vibration that is normally coupled into the resonator through the mounting structure will be reduced.

When considering all the factors that affect the two key parameters governing acceleration sensitivity, mainly the acoustic mode center position and the symmetry of the stress field, it is not surprising that a given batch of resonators will have such a wide spread in performance. For the stress field, its symmetry is dependent on the clip structure, the contour center, and the position of the blank within the crystal mount. For the acoustic mode, its center position is determined by the contour center, blank imperfections, and to a small degree the distribution of the stress field in the crystal blank. Designing a clip structure and manufacturing process to reduce the variation in all these factors is necessary to reduce acceleration sensitivity.

II. THE QUAD RELIEF MOUNT (QRM) STRUCTURE

The layout of the Quad Relief Mount (QRM) structure is illustrated in Fig. 1. It consists of a machinable ceramic base, a chemically etched lead-frame, and a quartz blank. The lead-frame is made of 0.1mm (0.004") thick ½ hard nickel-silver and it is formed to have support shelves that align and hold the crystal. The depth of the form controls the alignment of the crystal and lead-frame mid-planes.

[1] It has been recently stated that the acceleration sensitivity does not completely vanish, but in general, the effect is small compared to acceleration sensitivity caused by typical blank and mount imperfections, resonator misalignment, and other manufacturing process imperfections [4].

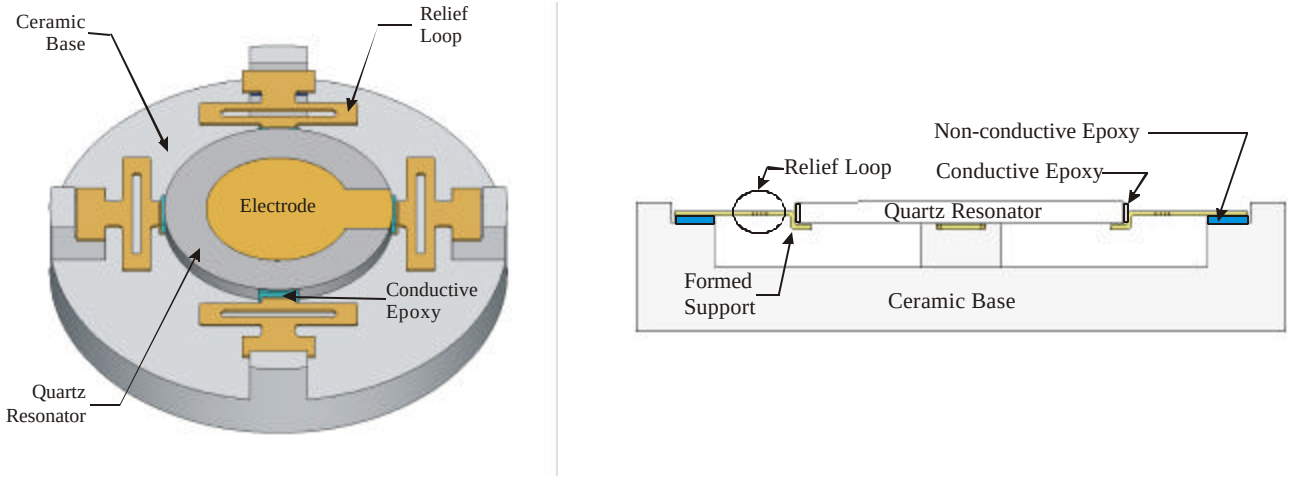

Fig. 1. Illustration of the Quad Relief Mount (QRM) structure demonstrating in-plane symmetry with compliance. (left) 3-D view and (right) front side section view. *note* Illustrations are not to scale.

The ceramic base provides a rigid, coplanar set of four points on which the lead-frame assembly can be mounted using a non-conductive epoxy. Once the epoxy cures, the unused portions of the lead-frame are cut away leaving the quad mount support structure shown. The crystal blank is then placed onto the formed supports using a conductive epoxy for support and electrical connections. The electrical connections are completed using bonding wire to the package pins (not shown).

III. Acceleration Sensitivity Measurement

For all the work described here, passive measurements were made without the use of an oscillator circuit. Using a custom circuit board fixture, the resonators were physically mounted onto the vibration table with a thin coaxial cable connecting it to a 180° hybrid transformer. On the balancing port of the hybrid a matched cable length with a capacitive trimmer is used to cancel out the C_0 of the resonator and the connecting cable. This is a convenient network as it gives a frequency response which is symmetrical about the series resonance. The signal source is an external synthesizer set to the crystal's series resonance. The relationship between the sideband levels and the acceleration sensitivity is defined by

$$\Gamma_i = \frac{\sqrt{4\omega_n^2 + \omega_3^2}}{\omega_0 a} \cdot 10^{\frac{L_i}{20}} \qquad (1)$$

where Γ_i is the component of acceleration sensitivity in the i direction, L_i is the sideband level in dBc, a is the g level, ω_v is the vibration frequency, ω_0 is the series resonant frequency, and ω_3 is the 3dB bandwidth of the crystal network. A vibration frequency of 70 Hz with a level of 10g peak acceleration was used to evaluate the resonators.

Two different acceleration sensitivity measurement methods were utilized, as described in [9-10]. The first method uses a network analyzer combined with a frequency source, which we will refer to as the network analyzer method. The second method used a phase detector, a lock-in amplifier, and a frequency source, and will be referred to as the lock-in method.

The acceleration sensitivity measurements were obtained by measuring along three mutually perpendicular axes [11]. For the two package styles used, one rectangular and the other circular, the acceleration sensitivity was measured as shown in Fig. 2. The acceleration sensitivity components are denoted by Γx, Γy, and Γz.

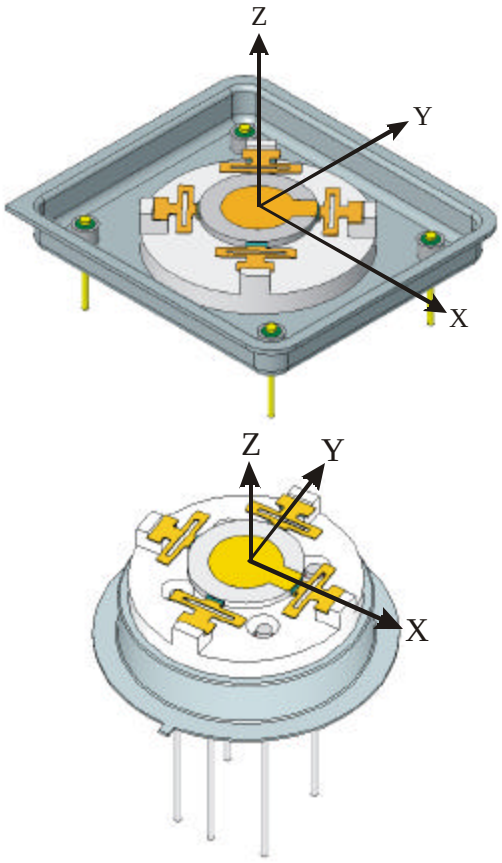

Fig. 2. Axial convention for the acceleration measurements.

IV. RESONATOR CONFIGURATIONS

Many variations of the Quad Relief Mount (QRM) structure were designed and tested. Both 8 and 10mm crystals, with and without flats, were used in this study. For the crystals without flats, the azimuthal orientations for the mounting locations were completely random. The crystal design parameters are listed in Table I. The initial experiments utilized unsealed resistance weld packages because of availability and cost. After the designs and packaging techniques were worked out, resonators were assembled and sealed into DDIL (26.2 x 23.8mm) cold weld packages. A smaller 8mm structure for the HC-40 cold weld package was also designed and tested.

To demonstrate the role of compliance on acceleration sensitivity, the Quad Stiff Mount (QSM) structure was designed without the relief loops.

TABLE I
CRYSTAL DESIGNS

Crystal Dia./Type	Plano-convex 10MHz 3rd overtone SC-cut			
	Contour Radius	Bi-Bevel Radius	Plateau Dia.	Electrode Dia./Material
8mm(no flats)	130mm	50.0mm	6.2mm	5.0mm Cr/Au
8mm(flats)	175mm	26.3mm	7.0mm	6.4mm Cr/Au
10mm(no flats)	240mm	50.0mm	7.6mm	6.5mm Cr/Au
10mm(flats)	525mm	26.3mm	9.0mm	7.4mm Cr/Au

V. RESULTS

A. Resistance Weld Quad Relief Mount Structure

Using resistance weld packages, the initial work was completed with 8 and 10mm crystals with flats (Figs. 3 and 4) and 10mm crystals with no flats (Fig. 5). The results are shown in Tables II and III, respectively. The best results were achieved with the 10mm crystals without flats. Surprisingly, the 10mm crystals with flats performed better than the 8mm crystals with flats. We believed that the higher acceleration sensitivity of the 8mm (with flats) structure was due, in part, to the longer sections of lead-frame between the crystal and the relief loops.

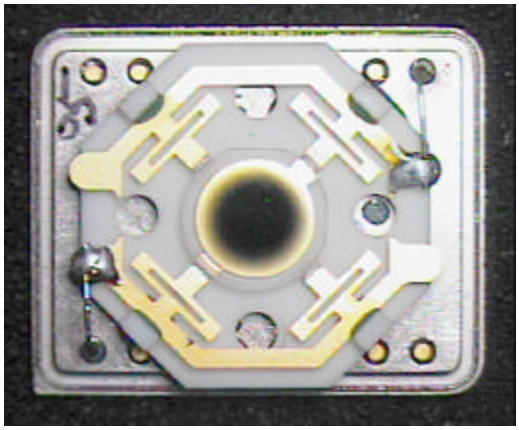

Fig. 3. (8mm) Resistance Weld QRM Structure (flats).

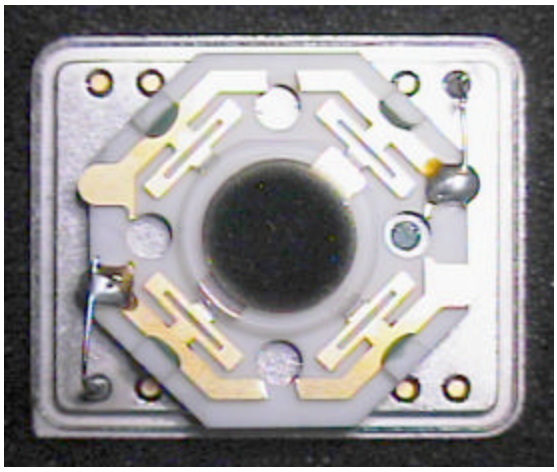

Fig. 4. (10mm) Resistance Weld QRM Structure (flats).

TABLE II
8 AND 10mm RESISTANCE WELD QRM STRUCTURES (FLATS)

Dev. #	$(10^{-9}/g)$			
	Γ_x [a]	Γ_y [a]	Γ_z [a]	$\lvert\Gamma\rvert$
8F-RW-QRM-1	0.14	0.23	0.05	0.27
8F-RW-QRM-2	0.05	0.33	0.05	0.34
8F-RW-QRM-3	0.13	0.16	0.16	0.26
8F-RW-QRM-4	0.18	0.74	0.06	0.76
8F-RW-QRM-5	0.22	0.36	0.21	0.47
8F-RW-QRM-6	0.04	0.36	0.26	0.45
8F-RW-QRM-7	0.13	0.28	0.08	0.32
Average				**0.41**
10F-RW-QRM-1	0.15	0.16	0.08	0.23
10F-RW-QRM-2	0.36	0.04	0.23	0.43
10F-RW-QRM-3	0.11	0.36	0.11	0.39
10F-RW-QRM-4	0.18	0.27	0.11	0.34
10F-RW-QRM-5	0.11	0.45	0.15	0.49
10F-RW-QRM-6	0.08	0.31	0.05	0.32
Average				**0.37**

[a] Measurements were taken using the network analyzer method.

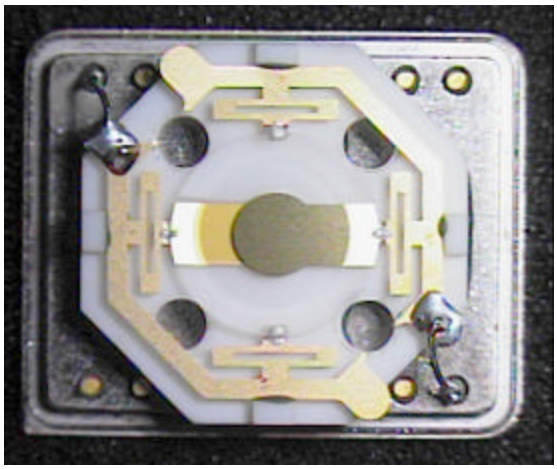

Fig. 5. (10mm) Resistance Weld QRM Structure (no flats).

TABLE III
10mm RESISTANCE WELD QRM STRUCTURES (NO FLATS)

Dev. #	(10^{-9}/g)			
	Γ_x [a]	Γ_y [a]	Γ_z [a]	$\lvert\Gamma\rvert$
10NF-RW-QRM-1	0.08	0.13	0.11	0.19
10NF-RW-QRM-2	0.09	0.11	0.12	0.19
10NF-RW-QRM-3	0.33	0.12	0.11	0.37
10NF-RW-QRM-4	0.09	0.12	0.08	0.17
10NF-RW-QRM-5	0.30	0.15	0.37	0.50
10NF-RW-QRM-6	0.09	0.17	0.12	0.23
10NF-RW-QRM-7	0.25	0.09	0.25	0.36
10NF-RW-QRM-8	0.10	0.10	0.13	0.19
Average				**0.27**

[a] Measurements were taken using the network analyzer method.

B. Resistance Weld Quad Stiff Mount Structure

To observe the role of compliance of the relief loops on g-sensitivity, some 8mm (Fig. 6) and 10mm (Fig. 7) QSM structures were assembled and tested. Shown in Table IV, the results were a few parts in 10^9 per g, an order of magnitude higher than the QRM structures.

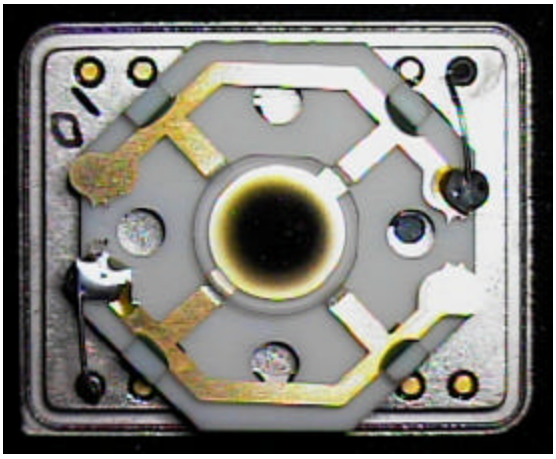

Fig. 6. (8mm) Resistance Weld QSM Structure (flats).

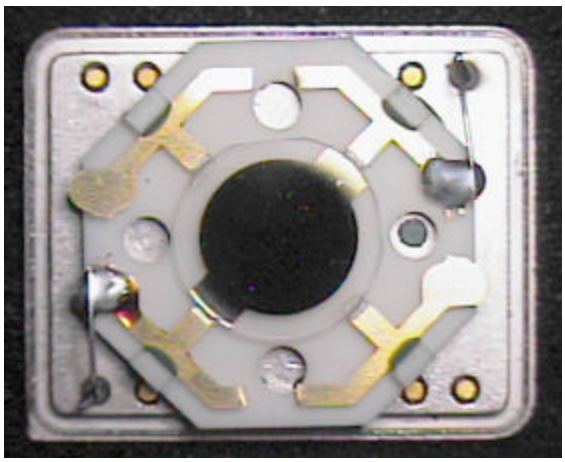

Fig. 7. (10mm) Resistance Weld QSM Structure (flats).

TABLE IV
8 AND 10mm RESISTANCE WELD QSM STRUCTURES (FLATS)

Dev. #	(10^{-9}/g)			
	Γ_x [a]	Γ_y [a]	Γ_z [a]	$\lvert\Gamma\rvert$
8F-RW-QSM-1	0.15	2.17	0.07	2.18
Average				**2.18**
10F-RW-QSM-1	0.29	1.98	1.70	2.63
10F-RW-QSM-2	1.15	2.00	1.52	2.76
10F-RW-QSM-3	0.48	1.52	2.87	3.28
Average				**2.89**

[a] Measurements were taken using the network analyzer method.

C. Mini-8mm Resistance Weld Quad Relief Mount Structure

A smaller 8mm design was laid out to be more like a scaled down version of the 10mm design (Fig. 8). This eliminated the longer sections of lead-frame between the crystal and the relief loops. Comparing the average acceleration sensitivity of this mini-8mm QRM structure with flats (Table V) to the 10mm QRM structure with flats (Table II), the smaller diameter crystal produced the lower average acceleration sensitivity.

To test the role of compliance once more, we assembled and tested an identical mini-8mm structure with no relief loops (Fig. 9). The results are shown in Table VI. Again we saw the order of magnitude difference between the QRM and QSM structures.

TABLE V
MINI-8mm RESISTANCE WELD QRM STRUCTURES (FLATS)

Dev. #	(10^{-9}/g)			
	Γ_x [a]	Γ_y [a]	Γ_z [a]	$\lvert\Gamma\rvert$
Mini-8F-RW-QRM-1	0.06	0.07	0.12	0.15
Mini-8F-RW-QRM-2	0.11	0.37	0.04	0.39
Mini-8F-RW-QRM-3	0.07	0.24	0.27	0.37
Mini-8F-RW-QRM-4	0.23	0.15	0.12	0.30
Average				**0.30**

[a] Measurements were taken using the network analyzer method.

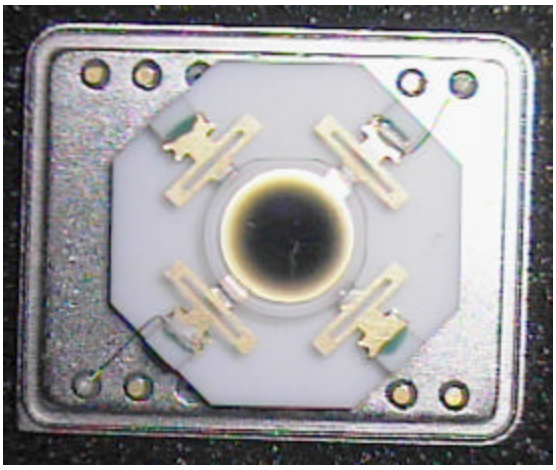

Fig. 8. Mini-8mm Resistance Weld QRM Structure (flats).

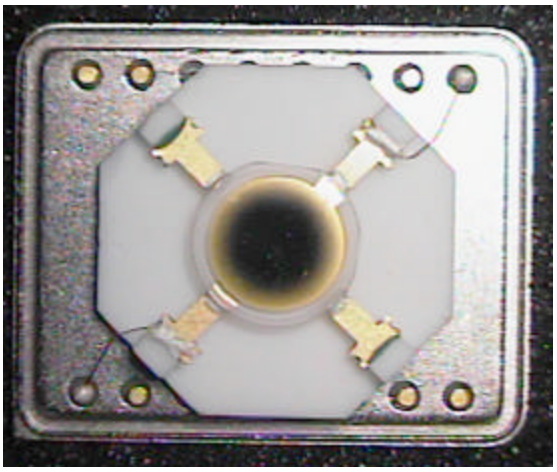

Fig. 9. Mini-8mm Resistance Weld QSM Structure (flats).

TABLE VI
MINI-8mm RESISTANCE WELD QSM STRUCTURES (FLATS)

Dev. #	(10^{-9} /g)			
	Γ_x [a]	Γ_y [a]	Γ_z [a]	$\lvert\Gamma\rvert$
Mini-8F-RW-QRM-1	1.68	0.54	1.57	2.36
Mini-8F-RW-QRM-2	2.01	0.20	3.29	3.86
Average				**3.11**

[a] Measurements were taken using the network analyzer method.

D. DDIL Cold Weld 8 and 10mm Quad Relief Mount

After the packaging techniques were worked out, numerous 8 and 10mm crystals (without flats) were assembled in DDIL (26.2 x 23.8mm) cold weld packages and sealed under vacuum (Figs. 10 and 11, respectively). The results were quite spread out, but there were some excellent performing resonators with acceleration sensitivities in the 10^{11} per g range (Table VII).

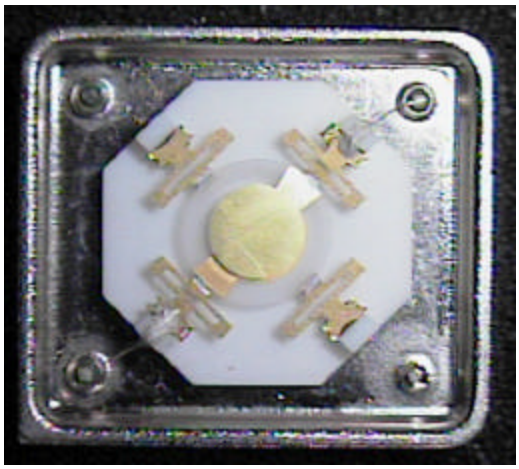

Fig. 10. Mini-8mm DDIL Cold Weld QRM Structure (no flats).

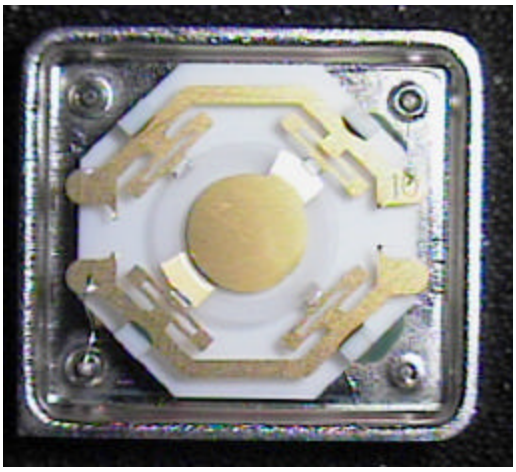

Fig. 11. (10mm) DDIL Cold Weld QRM Structure (no flats).

TABLE VII
MINI-8 AND 10mm DDIL COLD WELD QRM STRUCTURES (NO FLATS)

Dev. #	(10^{-9} /g)			
	Γ_x [b]	Γ_y [b]	Γ_z [b]	$\lvert\Gamma\rvert$
Mini-8NF-DD-QRM-01	-0.177	0.054	0.272	0.329
Mini-8NF-DD-QRM-02	-0.020	0.338	-0.116	0.358
Mini-8NF-DD-QRM-03	0.036	-0.138	-0.393	0.418
Mini-8NF-DD-QRM-04	-0.077	-0.015	-0.037	0.087
Mini-8NF-DD-QRM-05	-0.122	0.353	-0.630	0.732
Mini-8NF-DD-QRM-06	-0.170	-0.229	0.548	0.618
Mini-8NF-DD-QRM-07	-0.138	-0.078	-0.122	0.200
Mini-8NF-DD-QRM-08	-0.043	-0.055	-0.028	0.075
Mini-8NF-DD-QRM-09	0.203	-0.155	0.246	0.355
Mini-8NF-DD-QRM-10	0.177	-0.227	-0.308	0.422
Mini-8NF-DD-QRM-11	-0.201	-0.114	0.072	0.242
Mini-8NF-DD-QRM-12	-0.098	-0.052	-0.124	0.166
Mini-8NF-DD-QRM-13	-0.457	0.061	-0.076	0.467
Mini-8NF-DD-QRM-14	-0.150	-0.028	0.237	0.282
Mini-8NF-DD-QRM-15	0.229	0.023	0.278	0.361
Average				**0.341**
10NF-DD-QRM-01	0.309	0.119	-0.394	0.515
10NF-DD-QRM-02	-0.051	-0.341	-0.678	0.761
10NF-DD-QRM-03	-0.064	0.142	-0.139	0.209
10NF-DD-QRM-04	0.042	-0.033	-0.151	0.160
10NF-DD-QRM-05	0.023	-0.047	-0.114	0.125
10NF-DD-QRM-06	0.062	-0.176	0.678	0.703
10NF-DD-QRM-07	0.154	-0.200	-0.540	0.596
10NF-DD-QRM-08	-0.019	-0.030	0.123	0.128
10NF-DD-QRM-09	0.064	-0.067	-0.399	0.410
10NF-DD-QRM-10	0.176	-0.121	-0.310	0.376
10NF-DD-QRM-11	0.025	-0.017	0.031	0.043
10NF-DD-QRM-12	0.144	0.183	-0.290	0.372
10NF-DD-QRM-13	-0.015	-0.162	0.168	0.234
10NF-DD-QRM-14	0.209	-0.161	0.140	0.299
10NF-DD-QRM-15	0.015	0.025	-0.142	0.145
10NF-DD-QRM-16	0.129	-0.040	0.109	0.174
Average				**0.328**

[b] Measurements were taken with both the network analyzer and lock-in methods, but only the lock-in results are shown.

E. Mini-8mm HC-40 Quad Relief Mount Structure

The last design laid out was the HC-40 QRM structure. The first batch utilized part of the lead-frame structure to facilitate the electrical connections, (Fig. 12) while the second batch utilized bonding wires in order to prevent coupling of stress through the pins (Fig. 13). Batch #1 results are shown in Table VIII and batch #2 results are shown in Table IX. Both batches were sealed under vacuum.

The spread on the acceleration sensitivities is very good for the HC-40 QRM structures. For the first batch the range of values spanned from 0.15 to 0.46 parts in 10^9 per g, while for the second batch the range of values spanned from 0.08 to 0.30 parts in 10^9 per g. The average total Γ values were 0.29 and 0.19 parts in 10^{10} per g, respectively. Again we see two resonators in the high parts in 10^{11} per g range.

TABLE VIII
BATCH #1 Mini-8mm HC-40 COLD WELD QRM STRUCTURE (NO FLATS)

Dev. #	(10^{-9} /g)			
	Γ_x [a]	Γ_y [a]	Γ_z [a]	$\lvert\Gamma\rvert$
Mini-8NF-HC-QRM-01	0.15	0.15	0.29	0.36
Mini-8NF-HC-QRM-02	0.20	0.10	0.26	0.34
Mini-8NF-HC-QRM-03	0.10	0.10	0.26	0.30
Mini-8NF-HC-QRM-04	0.17	0.33	0.26	0.45
Mini-8NF-HC-QRM-05	0.09	0.09	0.08	0.15
Mini-8NF-HC-QRM-06	0.19	0.28	0.20	0.39
Mini-8NF-HC-QRM-07	0.07	0.12	0.14	0.20
Mini-8NF-HC-QRM-08	0.11	0.42	0.16	0.46
Mini-8NF-HC-QRM-09	0.08	0.13	0.10	0.18
Mini-8NF-HC-QRM-10	0.19	0.07	0.07	0.21
Mini-8NF-HC-QRM-11	0.33	0.15	0.12	0.38
Mini-8NF-HC-QRM-12	0.08	0.15	0.06	0.18
Mini-8NF-HC-QRM-13	0.16	0.12	0.08	0.22
Average				**0.29**

[a] Measurements were taken using the network analyzer method.

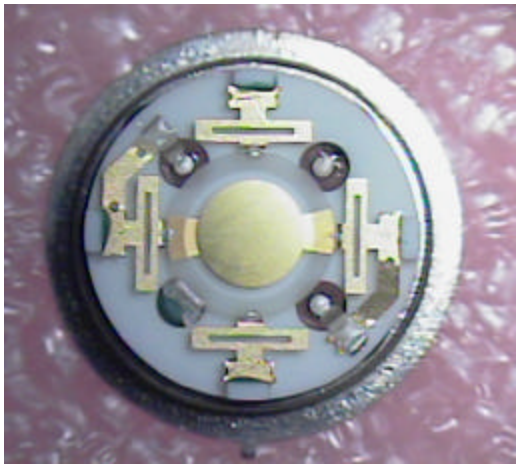

Fig. 12. Mini-8mm HC-40 Cold Weld QRM Structure (Batch #1).

TABLE IX
BATCH #2 Mini-8mm HC-40 COLD WELD QRM STRUCTURES (NO FLATS)

Dev. #	(10^{-9} /g)			
	Γ_x [c]	Γ_y [c]	Γ_z [c]	$\lvert\Gamma\rvert$
Mini-8NF-HC-QRM-14	-0.073	0.006	-0.263	0.273
Mini-8NF-HC-QRM-15	0.172	0.072	0.088	0.206
Mini-8NF-HC-QRM-16	0.086	-0.034	0.078	0.121
Mini-8NF-HC-QRM-17	0.037	0.030	-0.065	0.081
Mini-8NF-HC-QRM-18	-0.018	0.145	-0.069	0.162
Mini-8NF-HC-QRM-19	-0.059	0.063	0.014	0.087
Mini-8NF-HC-QRM-20	0.018	0.086	-0.242	0.257
Mini-8NF-HC-QRM-21	0.227	0.042	-0.185	0.296
Average				**0.185**

[c] Measurements were taken using the lock-in method.

Fig. 13. Mini-8mm HC-40 Cold Weld QRM Structure (Batch #2).

VI. DISCUSSION OF THE RESULTS

The results are summarized in Table X. First, it is very evident the role that the relief loops play on acceleration sensitivity. There is an order of magnitude difference between the QRM and QSM structures.

There are two possible reasons for this factor of ten improvement. The first possibility is the shape of the stress field. For the QSM structure there may be significant residual stresses present in the clip structure causing a distortion of the applied acceleration stress field. This, in turn, would result in a misalignment of the acoustic mode and stress field centers, and a corresponding degradation in acceleration sensitivity. For the QRM structure, the relief loops will allow the residual stresses to be reduced, returning the structure to a near zero stress bias. Since the geometry and in-plane symmetry of the QRM structure do not get grossly modified while the structure relaxes, the alignment of the acoustic mode and stress centers will still be very good.

The second possibility could be a frequency filtering effect, but a quick scan up to 2kHz showed no evidence of this. Further testing would be needed to confirm this.

TABLE X
ACCELERATION SENSITIVITY SUMMARY

Dia. (mm)	Total Γ (10^9 /g)				
	Device Type	Low	Ave.	High.	# tested
8	Res. Weld QRM (flats)	0.26	0.41	0.76	7
10	Res. Weld QRM (flats)	0.23	0.37	0.49	6
10	Res. Weld QRM (no flats)	0.17	0.27	0.50	8
8	Res. Weld QSM (flats)	-	2.18	-	1
10	Res. Weld QSM (flats)	2.63	2.89	3.28	3
mini-8	Res. Weld QRM (flats)	0.15	0.30	0.39	4
mini-8	Res. Weld QSM (flats)	2.36	3.11	3.86	2
mini-8	DDIL QRM (no flats)	0.08	0.34	0.73	15
10	DDIL QRM (no flats)	0.04	0.33	0.76	16
mini-8	HC-40 #1 QRM (no flats)	0.15	0.29	0.46	13
mini-8	HC-40 #2 QRM (no flats)	0.08	0.19	0.30	8

Looking at the various resistance weld QRM structures, the best performance was achieved by the 10mm crystal without flats. Intuitively this would be expected due to the enhanced symmetry of a resonator blank without flats. The second best performing resistance weld QRM was the smaller 8mm design.

The DDIL QRM structures and the second batch of HC-40 QRM structures had lower minimum acceleration sensitivities than were observed for the resistance weld QRM structures and the first batch of HC-40 QRM structures. There are a couple possible reasons for this.

First, it is worth noting that all the resistance weld structures and the first batch of HC-40 QRM structures were tested with the network analyzer method. After the development of the lock-in measurement technique, it was discovered that the network/spectrum analyzer had its own acceleration sensitivity which may have prevented the lower values from being resolved. Mainly, the network analyzer could only resolve to a lower limit of 1 to 2 parts in 10^{10} per g. It is possible that the better performing resistance weld and HC-40(Batch#1) structures had lower acceleration sensitivities than were measured. After isolating both measurement systems from the vibration table, the two methods corresponded very well [9].

Another possible factor in the lower acceleration sensitive resonators could be the sealing process. Sealing a lid onto the header may cause the overall package to become stiffer and more stable. For the DDIL package, the base and cover are identical except for the pins. When the two are cold welded together, the symmetry of the overall package is improved as compared to the resistance weld packages.

Finally, for the HC-40 resonators, the values are very low. For the second batch, all 8 of the resonators had acceleration sensitivities below 3 parts in 10^{10} per g. Two of the resonators were in the high parts in 10^{11} per g range.

Figure 14 shows the total Γ distribution for the sealed DDIL and HC-40 resonators. Although there is a significant spread of results on the 8 and 10mm DDIL cold weld structures, the lower limits were exceptional. For the 8mm DDIL, there were a couple of resonators in the high parts in 10^{11} per g range. For the 10mm structures, there was one resonator that had 4.3 parts in 10^{11} per g.

It is also interesting to note how the spread in the distribution decreases going from the DDIL package to the HC-40 package. The HC-40 structure is more compact and easier to assemble than the DDIL package. The placement of the ceramic base onto the center of the DDIL header is more difficult than for the HC-40 structure. Also notice how the distribution shifted to lower values going from the first to second batch of HC-40 structures.

VI. CONCLUSION

The QRM structure has reproducibly yielded resonators with low acceleration sensitivity. The advantages of the QRM structure over conventional packaging include in-plane symmetry and compliance. The role of compliance in the QRM structure has shown a factor of 10 improvement over an identical structure without compliance. It is believed that future enhancements of this structure will enable mid parts in 10^{11} to low parts in 10^{10} per g to be achieved easily and reproducibly.

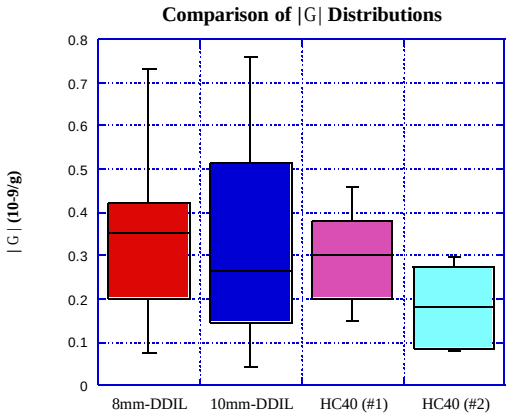

Fig. 14. Distribution of total Γ for the sealed QRM structures. The lower tick mark shows the lowest value, while the higher tick mark shows the highest value. The colored area represents the middle 50% of all the resonators in that batch and the line in the colored area represents the median value.

ACKNOWLEDGMENT

This work was supported by US Army contract # DAAB07-99-C-K764. The authors would like to thank Dr. John Vig of the US Army CECOM for useful discussions.

Thanks is also given to Mike Martin, Jim Buchanon, and Bharat Desai at Vectron International-Cinox and to Jacob Li at Vectron International-Norwalk for all their packaging assistance.

Additionally, thanks is given to Robin Potter, Steve Downing, Marke Cicero, and Daryl Killip for their contributions to the CAD, fabrication, and testing.

REFERENCES

[1] H.F. Tiersten and Y.S. Zhou, "The increase in the in-plane acceleration sensitivity due to its thickness asymmetry," *Proc. 45th Annual Symposium on Frequency Control*, pp. 289-297, 1991.

[2] H.F. Tiersten and Y.S. Zhou, "An analysis of the in-plane acceleration sensitivity of contoured quartz resonators with rectangular supports," *Proc. 44th Annual Symposium on Frequency Control*, pp. 461-467, 1990.

[3] Y.S. Zhou and H.F. Tiersten, "On the influence of a fabrication imperfection on the normal acceleration sensitivity of contoured quartz resonators with rectangular supports," *Proc. 44th Annual Symposium on Frequency Control*, pp. 452-460, 1990

[4] J.A. Kosinski and R.A. Pastore, Jr., "Implications of in-plane stretch and thickness compression coupled to flexure on the lower bound of BAW acceleration sensitivity," *Proc. 54th Annual Symposium on Frequency Control*, pp. 345-347, 2000.

[5] E.P. EerNisse, R.W. Ward, and O. Lew, "Crystal resonator with low acceleration sensitivity and method of manufacture thereof," U.S. Patent 5,168,191, December 1, 1992.

[6] E.P. EerNisse, L.D. Clayton, and M.H. Watts, "Distortions of thickness shear mode shapes in plano-convex quartz resonators with mass perturbations," *IEEE Transactions on Ultrasonics, Ferroelectrics, and Frequency Control*, vol. 37, no. 6, pp. 571-576, Nov. 1990.

[7] E.P. EerNisse, R.W. Ward, M.H. Watts, R.B. Wiggins, and O.L. Wood, "Experimental evidence for mode shape influence on acceleration-induced frequency shifts in quartz resonators," *IEEE Transactions on Ultrasonics, Ferroelectrics, and Frequency Control*, vol. 37, no. 6, pp. 566-570, Nov. 1990.

[8] R.D. Weglein, "The vibration-induced phase noise of a visco-elastically supported crystal resonator," *Proc. 43rd Annual Symposium on Frequency Control*, pp. 433-438, 1989.

[9] P.E. Morley and R.B. Haskell, "Method for measurement of the sensitivity of crystal resonators to repetitive stimuli," *Proc. 56th Annual Symposium on Frequency Control* (these proceedings).

[10] J.T. Stewart, P.E. Morley, and D.S. Stevens, "Theoretical and experimental results for the acceleration sensitivity of rectangular crystal resonators," *Proc. 53rd Annual Symposium on Frequency Control*, pp. 489-493, 1999.

[11] R. L. Filler, "The acceleration sensitivity of quartz crystal oscillators: a review," *IEEE Transactions on Ultrasonics, Ferroelectrics, and Frequency Control*, vol. 35, no. 3, pp. 297-305, May 1988.